

Available online at [www.sciencedirect.com](http://www.sciencedirect.com)

journal homepage: [www.elsevier.com/locate/AJPS](http://www.elsevier.com/locate/AJPS)

Original Research Paper

# Design and characterization of monolaurin loaded electrospun shellac nanofibers with antimicrobial activity <sup>☆</sup>



Nawinda Chinatangkul<sup>a,b,c</sup>, Chutima Limmatvapirat<sup>c,d</sup>,  
Jurairat Nunthanid<sup>b,c</sup>, Manee Luangtana-Anan<sup>b,c</sup>, Pornsak Sriamornsak<sup>b,c</sup>,  
Sontaya Limmatvapirat<sup>b,c,\*</sup>

<sup>a</sup> Faculty of Pharmacy, Siam University, Bangkok 10160, Thailand<sup>b</sup> Department of Pharmaceutical Technology, Faculty of Pharmacy, Silpakorn University, Nakhon Pathom 73000, Thailand<sup>c</sup> Pharmaceutical Biopolymer Group (PBiG), Faculty of Pharmacy, Silpakorn University, Nakhon Pathom 73000, Thailand<sup>d</sup> Department of Pharmaceutical Chemistry, Faculty of Pharmacy, Silpakorn University, Nakhon Pathom 73000, Thailand

## ARTICLE INFO

## Article history:

Received 5 November 2017

Accepted 18 December 2017

Available online 27 December 2017

## Keywords:

Shellac

Monolaurin

Nanofibers

Factorial design

Wound dressing

Electrospinning

## ABSTRACT

The aim of this study was to elucidate the optimized fabrication factors influencing the formation and properties of shellac (SHL) nanofibers loaded with an antimicrobial monolaurin (ML). The main and interaction effects of formulation and process parameters including SHL content (35%–40% w/w), ML content (1%–3% w/w), applied voltage (9–27 kV) and flow rate (0.4–1.2 ml/h) on the characteristic of nanofibers were investigated through a total of 19 experiments based on a full factorial design with three replicated center points. As a result, the SHL content was the major parameter affecting fiber diameter. Another response result revealed that the SHL content would be also the most significant negative impact on amount of beads. An increase in the concentration of SHL led to a reduction in the amount of beads. From the results of characterization study, it was proved that ML might be entrapped between the chains of SHL during the electrospinning process exhibiting an excellent encapsulation. According to the response surface area, small (7488 nm) and beadless (0.48) fibers were obtained with the SHL and ML contents of 37.5% and 1.1% w/w respectively, at the applied voltage of 18 kV and the flow rate of 0.8 ml/h. In addition, the results of the kill-kinetic studies showed that SHL nanofibers loaded with ML exhibited an excellent antibacterial activity against *Staphylococcus aureus*, while *Escherichia coli* was less affected due to the hydrophilic structure of its outer membrane. ML also exerted an antifun-

<sup>☆</sup> Peer review under responsibility of Shenyang Pharmaceutical University.

\* Corresponding author. Department of Pharmaceutical Technology, Faculty of Pharmacy, Silpakorn University, 6 Rachamankra Road, Ampur Mueng, Nakhon Pathom 73000, Thailand. Tel.: +66 34 255800.

E-mail address: [limmatvapirat\\_s@su.ac.th](mailto:limmatvapirat_s@su.ac.th) (S. Limmatvapirat).

Peer review under responsibility of Shenyang Pharmaceutical University.

gal activity by reducing the number of *Candida albicans* colonies. Based on their structural and antimicrobial properties, SHL nanofibers containing ML could be potentially used as a medicated dressing for wound treatment.

© 2017 Shenyang Pharmaceutical University. Published by Elsevier B.V.

This is an open access article under the CC BY-NC-ND license.

(<http://creativecommons.org/licenses/by-nc-nd/4.0/>)

## 1. Introduction

Wound is an injury which damages the skin, a protective barrier against the external environment. When a wound is exposed to the air, the scab, a crust of dried blood or serum, would be formed to cover the wound resulting in delayed wound healing [1]. Electrospun wound dressings work on the concept of moist wound healing which retains fluid contacting with wounds. The benefits of moist wound healing include inhibiting dry scab formation, decreasing the environment pH, affecting bacterial growth, shortening of the inflammatory phase of wound healing and providing an environment rich in enzymes, white blood cells and growth factors favorable for wound healing [2]. Due to their ultrafine network structures, electrospun nanofibers can be used for the replacement of extra cellular matrix (ECM) resulting in greatly rapid epithelialization and allowing the reduction of scar formation [3,4]. The porous nature of nanofibers dressings also enhances oxygen and nutrients transferring to cells leading to an increased healing rate [5]. In addition, they can improve drug loading capacity, and release rate because of their high surface to volume ratio properties [6].

With the aim of being placed in the biological and physiological environment of a wound, nanofibers are mostly developed from biopolymers. SHL is a nontoxic natural polymer secreted by the lac insect, on some specific trees mainly in China, India and Thailand. There were few studies on the application of SHL in wound healing management, especially through electrospinning process [7]. Currently, SHL is widely used for enteric coating to protect drugs from acid degradation in the gastrointestinal tract and fruit coating to prevent microbial entry and water loss [8–10]. Due to the excellent film forming and protective properties, electrospun shellac nanofibers could be used as potential wound dressings.

Infection might cause a delay in wound healing. To prevent the multiplication of pathogens, an antimicrobial agent should be incorporated. Apparently, antibiotic resistance has become an increasing worldwide problem for infection treatment. Therefore, safe and effective antimicrobials which are not easily subject to resistance are greatly required. Among these simple antimicrobial compounds, natural lipids seem to be an achievable choice [11]. Fatty acids and their corresponding esters might have little or no toxicity and also exert antimicrobial activity. Isaacs, Litov and Thormar (1995) found that fatty acids and monoglycerides with medium chain lengths yielded more biologically active than long chain monoglycerides in killing viruses and bacteria [12]. Among medium chain fatty acids (C8 to C14), lauric acid (C12) has more antimicrobial activity than other fatty acids such as

myristic acid (C14), capric acid (C10) or caprylic acid (C8) [13]. It could be found in human breastmilk, skin surface and other natural foods such as coconut oil and palm kernel oil [13]. ML, known as glycerol monolaurate, is a monoester form of lauric acid. It has many times greater antibacterial and antiviral activity than lauric acid. Tangwacharin and Khopaibool (2012) revealed that minimum bactericidal concentrations (MBC) of lauric acid and ML were 3.2 mg/ml and 0.1 mg/ml, respectively [14]. The lower MBC value of ML indicated the stronger antimicrobial activity than that of lauric acid. ML has Generally Recognized As Safe (GRAS) status considered to be nontoxic [13]. It is approved in the US as a food emulsifier and has been used to control growth of pathogenic organisms and spoilage in food processing industries [15]. ML exhibits a broad-spectrum bactericidal activity against Grampositive bacteria from superficial skin infections and also has an antifungal effect by inhibiting spore germination and preventing the radial growth [13,16–18]. Previous studies revealed that the topical use of ML could inhibit the growth of *Staphylococcus aureus*, a significant cause of skin and mucosal infections [18]. Besides the killing effect, ML might stabilize mucosal and skin surfaces, thus avoiding inflammation and further infection [18]. In addition to *S. aureus*, *Streptococcus pyogenes*, *Clostridium perfringens*, *Mycobacterium terrae*, *Listeria monocytogenes*, *Streptococcus agalactiae*, and Groups C, F, and G streptococci could be killed by ML [13,18]. Fungi, yeast, and protozoa were also reported to be inactivated by ML. *Candida albicans*, an opportunistic human yeast pathogen found in the oral pharynx, gut, genitourinary tract and skin, was potentially affected by ML [19]. Additionally, the development of microbial resistance to ML was also considered rare to occur [18]. However, there are few studies exploring the possibility of ML as an alternative antimicrobial agent in the pharmaceutical dosage forms, including wound dressing.

The morphology of electrospun nanofibers and other related properties could be affected by various parameters which are broadly divided into formulation parameters, process parameters and ambient parameters [20]. Experimental design techniques have been applied to determine the main effects and interaction between parameters, and also to reduce development time and the numbers of experimental trials [21].

The aims of this research were to investigate which factors (SHL and ML concentrations, applied voltage and flow rate) and interaction effects between these factors would have the most impact on the morphology of SHL nanofibers loaded with ML as well as the interaction among these factors. The fabrication conditions were optimized by using a full factorial design with three replicated center points. Various instrumental analyses including powder X-ray diffraction, differential

scanning calorimetry and FTIR spectroscopy were also employed in order to investigate the physicochemical characteristics of ML in SHL matrix.

## 2. Materials and methods

### 2.1. Materials

SHL (Lot No. 55) and ML (Lot No. 150520) were purchased from Mahachai Shellac Part., Ltd. (Samut Sakhon, Thailand) and Shanghai Terppon Chemical Co., Ltd., respectively. The following microbial strains obtained from Department of Medical Sciences, Thailand were performed in the antimicrobial assay: *S. aureus* DMST 8013, *Escherichia coli* DMST 4212 and *C. albicans* DMST 5815. The media including tryptic soy broth and agar (TSB, Lot No. VM229958 and TSA, Lot No. VM221159) were purchased from Merck KGaA (Germany) and sabouraud dextrose broth and agar (SDB, Lot No. VM331339 and SDA, Lot No. 3200237) were purchased from Merck KGaA (Germany) and Becton, Dickinson and Company (USA), respectively. Sterile powders of streptomycin (Lot No. 9/2015) and ketoconazole (Lot No. KT/14/08/18514) were obtained from General Drugs House Co., Ltd. and Greater Pharma Co., Ltd., respectively, and used as positive controls for antimicrobial test. Ethanol (95% v/v) used as a solvent for preparing spinning solutions was of reagent grade.

### 2.2. Physicochemical characterization of monolaurin loaded shellac films and fibers

The SHL-based polymeric films containing different concentrations of ML were initially prepared by dissolving definite amount of SHL (40% w/w) and varied amounts of ML in the range of 3%–15% w/w in 95% v/v ethanol under overnight stirring at room temperature followed by solvent evaporation. The highest level of ML loading in the obtained films was accordingly analyzed using powder X-ray diffraction (PXRD). Consequently, SHL nanofibers loaded with the maximum amount of incorporated ML were fabricated and further evaluated for the physicochemical characteristics using powder X-ray diffraction (PXRD), differential scanning calorimetry (DSC) and Fourier transformed infrared spectroscopy (FTIR).

#### 2.2.1. Powder X-ray diffraction (PXRD)

The crystalline or amorphous characteristic of the samples was evaluated using powder X-ray diffractometer (MiniFlex II, Rikaku, Japan). The scan was performed at 30 kV and 15 mA in the  $2\theta$  range of  $5^\circ$  to  $40^\circ$  with the speed of  $4^\circ/\text{min}$  using Cu  $K\alpha$  radiation ( $\lambda = 0.154 \text{ nm}$ ).

#### 2.2.2. Differential scanning calorimetry (DSC)

The thermal characteristic of materials was investigated using differential scanning calorimeter (Sapphire, Perkin Elmer, Germany) under nitrogen gas flow with the rate of 20 ml/min. Samples were sealed in standard liquid aluminum pans and heated from 25 to 200 °C with the rate of 10 °C/min.

#### 2.2.3. Fourier transformed infrared spectroscopy (FTIR)

The molecular behavior and interaction of ML in SHL matrix was examined using FTIR spectrophotometer (Nicolet

Avatar 360, USA). During the process, each sample was ground and triturated with dry potassium bromide (KBr), and consequently compacted by hydraulic press machine to form pellet. The obtained pellet was placed in the sample holder. The scan was processed from 4000 to  $400 \text{ cm}^{-1}$  at  $4 \text{ cm}^{-1}$  resolution. The FTIR spectrum of each sample was obtained and analyzed using the OMNIC FTIR software.

### 2.3. Fabrication of monolaurin loaded shellac fibers through electrospinning process

#### 2.3.1. Preparation and evaluation of shellac-monolaurin solutions

The solutions at selected SHL-ML ratios were prepared by dissolving finely ground SHL and ML in 95% v/v ethanol and then magnetically stirring for overnight at room temperature before adjusting to the desired content. In order to eliminate insoluble contamination, the homogenous solution was centrifuged at 8000 rpm for 30 min. The obtained solution was further subjected to study solution property, and fiber morphology after fabrication via electrospinning process.

The properties of SHL-ML solutions including viscosity, surface tension and conductivity were examined by rheometer (Malvern Kinexus, UK), drop shape instrument (FTA 1000, USA) and electrical conductivity meter (Exttech EC500, USA), respectively.

#### 2.3.2. Preparation and evaluation of shellac-monolaurin fibers

In this process, each SHL solution with ML was filled in a syringe linked with a high-voltage power supply. An electric field was performed between the metallic needle tip of the syringe and the collector. When the voltages were applied, nanofibers were then produced on the surface of a target drum wrapped with an aluminum sheet which stored at the controlled conditions (23–26 °C and 40%–60% RH). The morphology of the obtained fibers was investigated using scanning electron microscope (SEM) (LEO 1450 VP, UK). Based on SEM images, J Micro-Vision 1.2.7 software was utilized to measure the diameter of the fibers and the amount of beads. The influence of independent factors; formulation and process parameters including viscosity, surface tension, conductivity, applied voltage and feed rate, on the morphological characteristics of fibers were determined in order to find the significant factors for further design of experiment.

### 2.4. Experimental design

A  $2^4$  full factorial design with three replicates at the center point was performed in order to find the optimized significant independent factors for the multiple responses of fiber properties. The diameter of fibers and the amount of beads (bead-to-fiber ratio) were the observed responses. The critical variables and their levels considered in the design of experiment are shown in Table 1. The Design Expert 8.0.4 software (Stat-Ease Inc., USA) was used for the analysis of the resultant data. In addition, the optimum conditions for the fabrication of nanofibers with desired morphology were also determined.

**Table 1 – Experimental range and levels of independent parameters.**

Parameters	Symbol	Variable levels		
		Low (-1)	Central point (0)	High (+1)
SHL content [% w/w]	X <sub>1</sub>	35.0	37.5	40.0
ML content [% w/w]	X <sub>2</sub>	1.0	2.0	3.0
Applied voltage [kV]	X <sub>3</sub>	9.0	18.0	27.0
Flow rate [ml/h]	X <sub>4</sub>	0.4	0.8	1.2

## 2.5. Time-kill kinetics

Time-kill assays were performed in order to study the pharmacodynamics of antimicrobial agents, showing a profile of antimicrobial activity over time. Prior to the kinetic test, *S. aureus* and *E. coli* were cultured in TSB media. Whereas *C. albicans* were cultured in SDB media. After overnight incubation at 37 °C, the density of inoculation was further diluted to 10<sup>4</sup> CFU/ml. For the kinetic test, 30 min UV-sterilized SHL nanofibers loaded with ML and ML in a solution form were added in the media broth to give the same final concentration of ML (2 mg/ml). SHL fibers without ML were used as the negative control, while streptomycin and ketoconazole were used as positive controls for antibacterial and antifungal test, respectively. All tubes were shaken and incubated at 37 °C. At different time points (0, 15, and 30 min, 1, 3, 6 and 9 h), 100 µl of each sample was taken and spread on a media agar. All plates were then incubated for 24 h at 37 °C. The number of colonies was counted and calculated for the percentage of living microbial cells as following equation.

$$\text{The percentage of living microbial cells} = (C_t \times 100)/C_0 \quad (1)$$

where C<sub>0</sub> and C<sub>t</sub> are the number of colonies at initial time (before adding the sample) and each time point, respectively.

## 3. Results and discussion

### 3.1. Evaluation of physical state and compatibility of the components in monolaurin loaded shellac matrix

The physicochemical characterizations of ML loaded SHL matrix including crystallinity property, thermal characterization and molecular behavior and interaction were determined by using PXRD, DSC and FTIR as described below.

#### 3.1.1. Powder X-ray diffractometry (PXRD)

The PXRD patterns of SHL powder, ML powder, their physical mixture, nanofibers and films in the weight ratio of 40:3 are illustrated in Fig. 1. The crystalline peaks as indicated by the diffraction peaks at 2θ values of 9.6°, 19.6°, 20.5° and 23.0° were clearly observed in the PXRD pattern of ML powder while SHL powder was in amorphous state as presented in a halo PXRD pattern. After encapsulation of ML in SHL nanofibers or films, the characteristic crystalline peaks of ML were absent

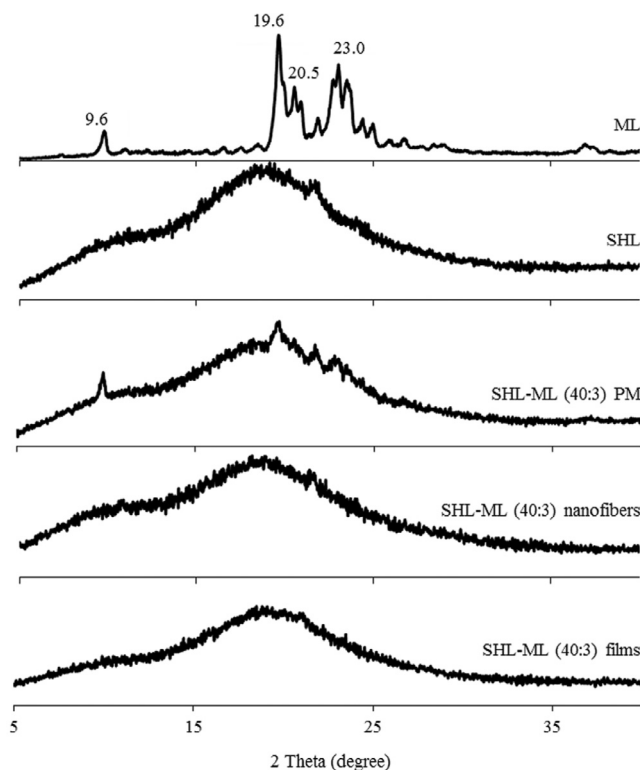


**Fig. 1 – Powder X-ray diffraction patterns of SHL, ML, their physical mixture, nanofibers and films in the weight ratio of 40:3.**

assuming that ML might be entrapped in the SHL matrix. It was also noted that fast drying rate during electrospinning was not the cause of disappearance of ML diffraction peak (amorphization) since slow evaporation during the film casting also demonstrated the similar PXRD pattern as that obtained from electrospinning. In this case, the ML molecules should be molecularly dispersed among the polymer chains of SHL, resulting in the disappearance of crystalline structure.

The SHL films containing various amounts of ML were developed aiming to investigate the highest level of incorporated ML. Based on Fig. 2A, the diffraction peaks due to crystalline ML were clearly observed in the PXRD patterns of all SHL-ML physical mixtures, especially at high fraction of ML. However, the peak intensity due to ML in PXRD patterns of SHL-ML films (Fig. 2B) became obviously decreased as compared to that of the corresponding physical mixtures. According to the PXRD profiles of SHL-ML films at the ratios of 40: 5 and 40: 3, the diffraction peaks completely disappeared and changed to halo pattern, suggesting the complete encapsulation or monomolecular dispersion of ML into SHL matrix films at these ratios. Thus, the suitable ratio of SHL to ML should be 40: 5 in which ML could be completely loaded in SHL nanofibers. Nevertheless, after preliminary investigation by electrospinning process, nanofibers containing 40: 5 weight ratio of SHL to ML could not be performed because of tackiness. Therefore, the combination of SHL with ML at the ratio of 40: 3 was found to be the maximum loading amount of ML.

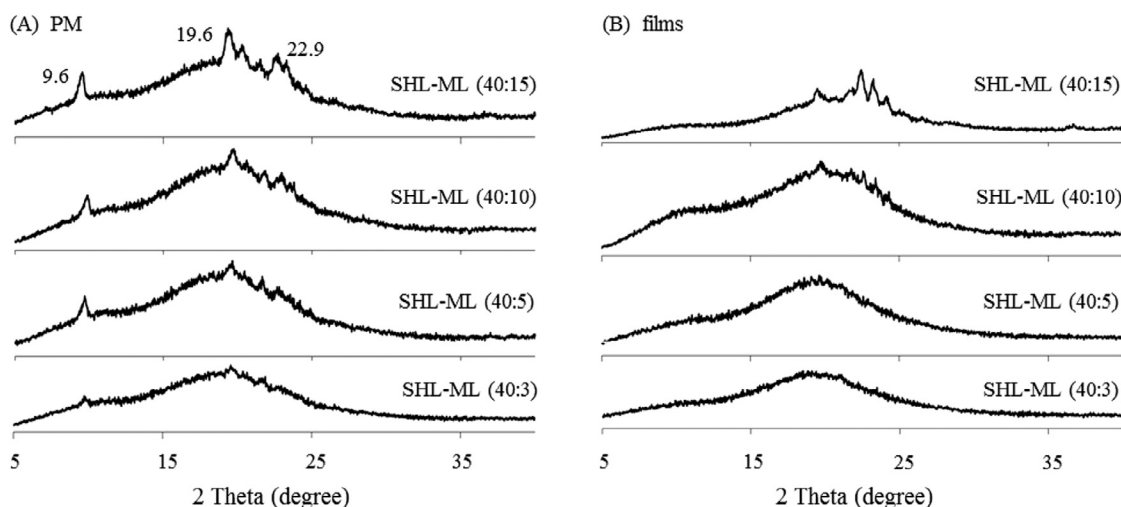


**Fig. 2 – Powder X-ray diffraction patterns of (A) SHL-ML physical mixtures with different amounts of ML and (B) their corresponding films.**

### 3.1.2. Differential scanning calorimetry (DSC)

DSC is one of the common tools for studying the interaction between the active drug and excipients and also assessing the possible incompatibilities which is significantly involved in the dosage form development [22]. In this study, DSC was employed to study the interaction between SHL and ML. The DSC thermograms of SHL, ML and their corresponding samples are illustrated in Fig. 3. Based on the DSC curve of ML, a large endothermic peak was obtained at about 66 °C indicating the melting temperature of ML. Meanwhile, pure SHL displayed the melting peak at about 69 °C which was almost the same position as ML. The physical mixture showed the broad endothermic peak, presumably due to the overlapped melting peaks of ML and SHL, at 68 °C. However, the films and nanofibers demonstrated the different results as compared to those found in the physical mixture. The loss of endothermic peaks of ML and SHL was obviously observed in the DSC

thermograms of the films and nanofibers which suggested the strong interaction between SHL and ML. The ML crystals might be changed from crystal state to molecular level and interacted with polymer structure of SHL during processing which was in accordance to the XRD results.

### 3.1.3. Fourier transform infrared spectroscopy (FTIR)

In order to provide more insight into the chemical interaction between components, FTIR was used for studying the molecular behavior of ML in SHL matrix. As illustrated in Fig. 4, ML showed a broad peak with the maxima around  $3314\text{ cm}^{-1}$  which was assigned as O–H stretching of the hydroxyl groups at the glycerol backbone while the peaks at  $1731$  and  $1182\text{ cm}^{-1}$  were attributed to carbonyl (C=O) stretching and C–O stretching of lauryl ester, respectively [23]. SHL also demonstrated the peak due to O–H stretching of hydroxyl groups and C=O stretching but in the different posi-

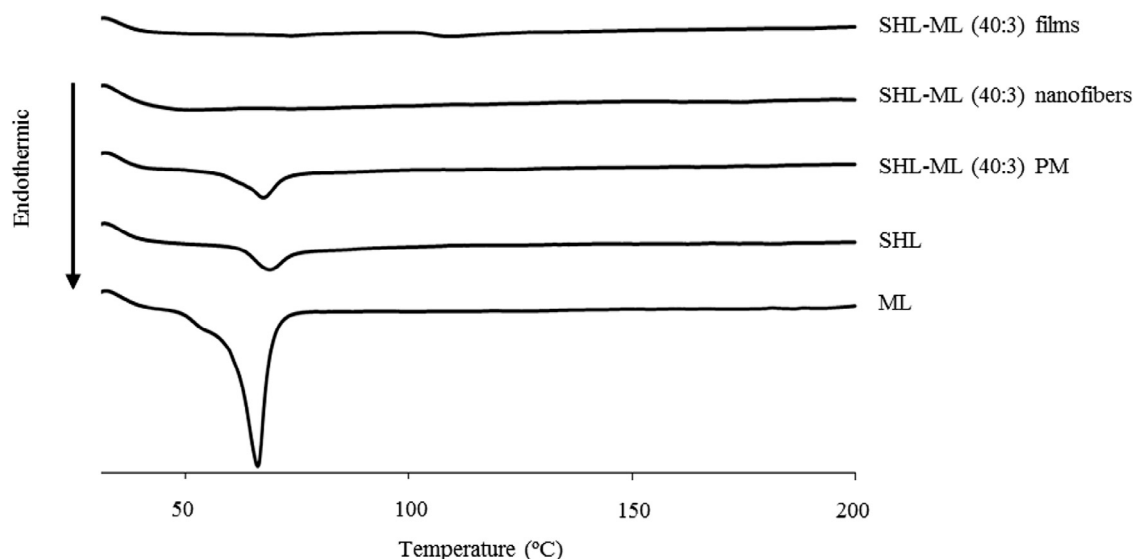


**Fig. 3 – DSC thermograms of SHL, ML, their physical mixture, nanofibers and films in the weight ratio of 40:3.**

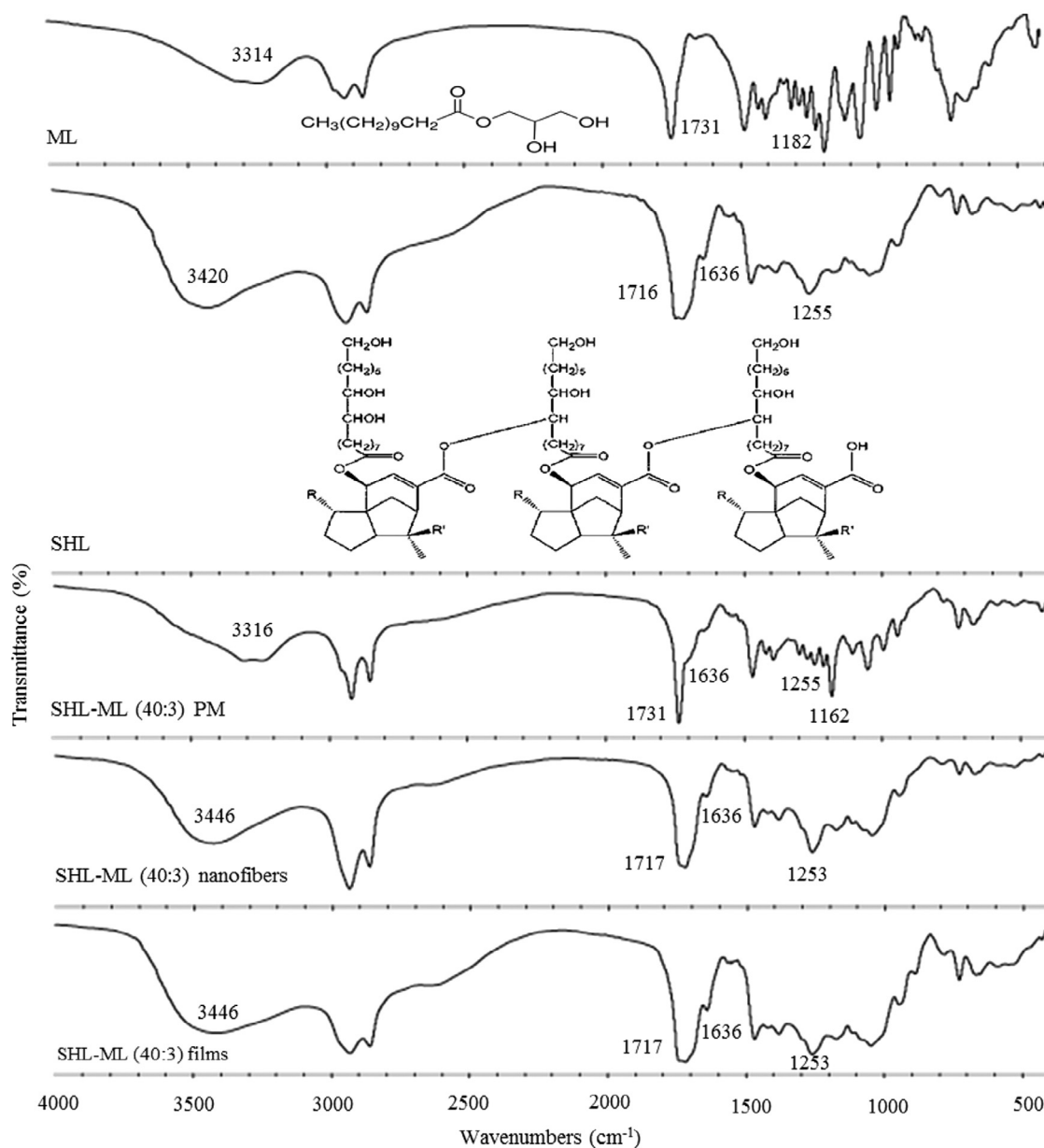


**Fig. 4 – FTIR spectra of SHL, ML, their physical mixture, nanofibers and films in the ratio of 40: 3.**

tions of  $3420\text{ cm}^{-1}$  and  $1716\text{ cm}^{-1}$ , respectively. Additionally, the peaks assigned to alkenyl ( $\text{C}=\text{C}$ ) and  $\text{C}-\text{O}$  stretching band were observed at  $1636$  and  $1255\text{ cm}^{-1}$ , respectively [24]. For the physical mixture, the superimposed spectrum between SHL and ML was observed. However, the FTIR spectrum of ML loaded SHL fibers was clearly changed as compared to that of the physical mixture. After the incorporation of ML into SHL fibers, the shift of broad  $\text{O}-\text{H}$  bands of ML ( $3314\text{ cm}^{-1}$ ) and SHL ( $3420\text{ cm}^{-1}$ ) to the maxima around  $3446\text{ cm}^{-1}$  was observed while the peaks assigned to  $\text{C}=\text{O}$  stretching of ML ( $1731\text{ cm}^{-1}$ ) and SHL ( $1716\text{ cm}^{-1}$ ) were shifted to  $1717\text{ cm}^{-1}$ . Additionally, the peak intensity of ML was clearly decreased after loading into the SHL fibers. Besides, a characteristic peak assigned to  $\text{C}=\text{C}$  stretching ( $1636\text{ cm}^{-1}$ ) of SHL in SHL-ML fibers was not changed which suggested that only some functional groups of SHL was involved in the interaction. Similar results were

observed in the FTIR spectrum of SHL-ML films and therefore confirmed the specific interaction between SHL and ML after incorporation into the matrix of either SHL fibers or films. In this case, the intermolecular hydrogen bonding among the hydroxyl groups and carbonyl groups of SHL and ML might be a possible explanation.

### 3.2. Evaluation of SHL-ML solution properties

The solution property might play a significant role in the electrospinning process affecting the morphology of the obtained nanofibers. During the electrospinning process, the solution was ejected from the needle tip depending on the stretching capacity of the solution which would be influenced by conductivity, viscosity and surface tension [20]. Obviously, as illustrated in Table 2, the increased concentration of SHL led to

**Table 2 – Effect of SHL and ML concentrations on the solution properties.**

SHL content (% w/w)	ML content (% w/w)	Solution properties		
		Viscosity (mPa·s)	Conductivity ( $\mu$ S)	Surface tension (mN/m)
35.0	1.0	454.2	26.41	2.24
35.0	2.0	335.4	26.33	2.18
35.0	3.0	251.5	26.29	2.16
37.5	1.0	676.7	23.75	2.20
37.5	2.0	561.9	23.27	2.21
37.5	3.0	411.8	23.05	2.13
40.0	1.0	750.8	22.23	2.24
40.0	2.0	705.3	20.97	2.18
40.0	3.0	643.4	20.64	2.16

a remarkable increase in viscosity, a slight decline in conductivity, but no significant change in surface tension. The viscosity was directly related to SHL content. As the concentration of SHL was increased, the amount of polymer chain entanglement was also increased resulting in a significant elevation in viscosity [20]. Generally, SHL is a non-ionic polymer with dielectric constant ( $\epsilon$ ) of 3.6 [25]. When the SHL content was increased, the electrical conductivity of a solution seemed to decline as a result of the decreased charge carrier mobility. Meanwhile, the surface tension of a solution was not significantly different. This could be explained by the dispersed distribution of SHL molecules in the solution which was not projected to the surface.

In addition, the introduction of ML into the SHL solutions could also affect the solution properties. When the content of ML was increased, the solution tended to have a slight reduction in viscosity which was presumably owing to the change in chain conformation of SHL. As discussed earlier, ML could be entrapped between the chains of SHL during the process of electrospinning, thus reducing the entanglement of SHL chains and resulting in a slight decrease in viscosity. A slight decrease in conductivity might be induced by an increase in the amount of ML due to the non-ionic property of ML [26]. However, the surface property of a solution was not changed after incorporating ML in the same manner as described above.

### 3.3. Experimental design

The morphology of electrospun nanofibers could be influenced by various parameters including formulation parameters, process parameters and ambient parameters [20]. As mentioned earlier, the solution property could affect the stretching capacity of the solution leading to the change of fiber morphology. Besides, studying all of the parameters in a single framework simultaneously seemed to be impossible and therefore needed the experimental design to reduce the number of experimental trials [21]. In this work, a two-level full factorial design along with three replicates at the center point was adopted in order to evaluate all possible combinations of parameter levels providing an accurate interpretation, along with an experimental error estimate [21]. Refer-

**Table 3 – Full factorial design and experimental responses for each design point.**

Run	X <sub>1</sub>	X <sub>2</sub>	X <sub>3</sub>	X <sub>4</sub>	Fiber diameter (Y <sub>1</sub> ) [nm]	Bead amount (Y <sub>2</sub> )
1	-1	-1	-1	-1	297	0.76
2	+1	-1	-1	-1	554	0.05
3	-1	+1	-1	-1	378	1.04
4	+1	+1	-1	-1	741	0.02
5	-1	-1	+1	-1	309	0.80
6	+1	-1	+1	-1	774	0.03
7	-1	+1	+1	-1	448	1.04
8	+1	+1	+1	-1	695	0.02
9	-1	-1	-1	+1	315	1.20
10	+1	-1	-1	+1	714	0.16
11	-1	+1	-1	+1	549	0.43
12	+1	+1	-1	+1	830	0.03
13	-1	-1	+1	+1	357	0.96
14	+1	-1	+1	+1	783	0.03
15	-1	+1	+1	+1	544	0.42
16	+1	+1	+1	+1	888	0.03
17	0	0	0	0	394	0.75
18	0	0	0	0	411	0.65
19	0	0	0	0	335	0.78

ring to the results obtained from preliminary experiments, the most significant factors affecting the morphology of electrospun nanofibers were the contents of SHL (X<sub>1</sub>) and ML (X<sub>2</sub>), applied voltage (X<sub>3</sub>) and flow rate (X<sub>4</sub>). Meanwhile, some variables might be held constant. In this procedure, the distance between the tip and collector was maintained at 20 cm. The process of electrospinning was conducted at the controlled conditions (23–26 °C and 40%–60% RH). In addition, the desired level of each factor was selected. Due to preliminary investigation, the concentration of SHL should be between 35% and 40% w/w. With the reduced content of SHL below 35% w/w, polymeric beads were generated instead of continuous fibers, and with the increased amount of SHL above 40% w/w, the nanofibers could not be fabricated resulting from the hard ejection of polymer solution. The optimum concentration of ML was in a range of 1% to 3% w/w. At a content of ML above 3% w/w, the loaded nanofibers found to be liquefied. In case of processing parameters, the effective range of applied voltages for the fabrication process was between 9 and 27 kV. The high voltages (over 27 kV) might produce electrical arcs, while the drawing capacity of polymer solution from the tip was poor with the applied voltages below 9 kV. The appropriate flow rate was in a range of 0.4 to 1.2 ml/h.

#### 3.3.1. Effects of the independent parameters on the morphology of SHL-ML nanofibers

A series of 19 experiments based on a 2<sup>4</sup> full factorial design with three replicated center points was performed (Table 3). Pareto charts were presented via a series of ordered bar graphs in order to determine the most significant factors and their interactions. In the presented plot, there were two different t limits including the Bonferroni-corrected t and the standard t. The factor effects might become certainly significant as presented above the Bonferroni limit. The effects were possibly significant as displayed above the t value limit while the influ-

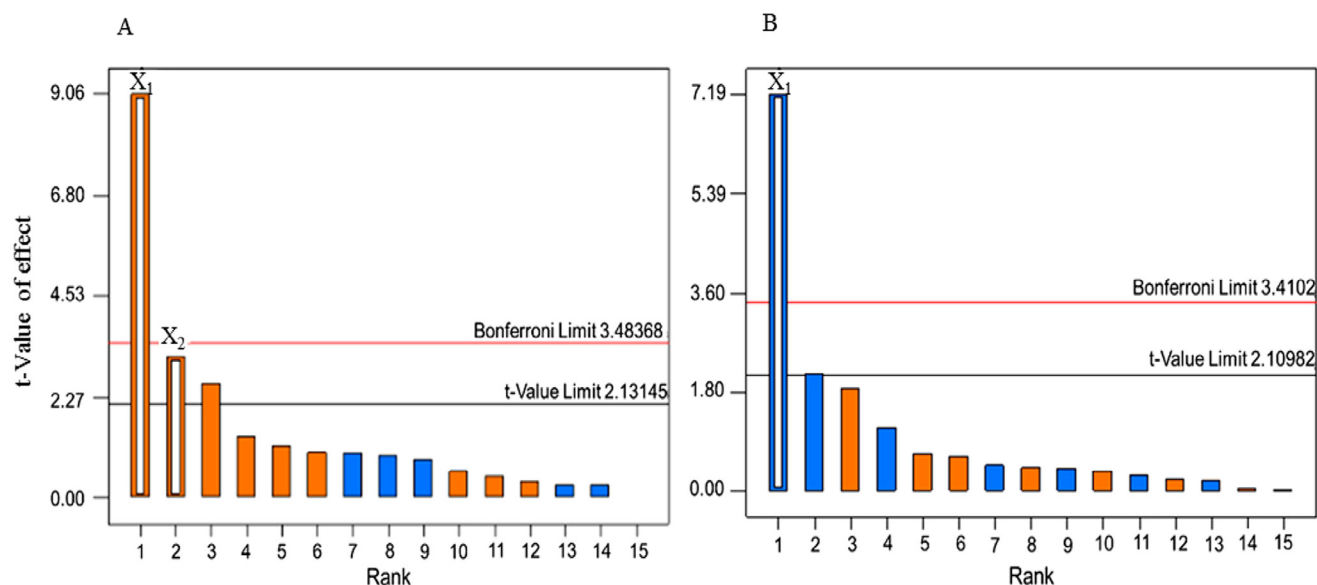


Fig. 5 – Pareto charts of the response values of (A) nanofiber diameter and (B) bead amount.

ences seemed to be not significant as shown below the t value limit [27]. As demonstrated in Fig. 5A and Fig. 6, Pareto charts and the diameter distributions of nanofibers at different concentrations of SHL and ML revealed that the SHL content ( $X_1$ ) had a tremendous effect on the diameter of fibers while the ML level ( $X_2$ ) was the minor factor. For examples, electrospun fibers prepared from 40% w/w SHL (Fig. 6D, 6E) indicated the larger diameter as compared to those prepared from 35% w/w SHL with the same concentration of ML (Fig. 6A, 6E). Similarly, the electrospun fibers prepared from a higher concentration of ML (Fig. 6A, 6B) demonstrated the larger fiber size as compared to those prepared from a lower concentration of ML (Fig. 6D, 6E) although less extent was observed. As mentioned earlier (Table 2), the increased concentration of SHL resulted in the significant increase of viscosity and the slight decrease of conductivity leading to a reduction in the stretching capacity of the solution. As a result, nanofibers with large diameters might be obtained [20]. Another factor affecting the fiber diameter was the concentration of ML. Based on theoretical expectation, an increase in the viscosity of electrospun solution contributes to an increase in the resultant fiber di-

ameter due to a decrease in the stretching capacity during the electrospinning process [20]. By contrast, the fabricated nanofibers appeared to be thicker with the presence of increased ML, although the reduced viscosity was clearly indicated. In this case, the influence of viscosity as well as the stretching capacity might be presumably dominated by another factor. As explained in the section 3.1, the possible interaction between SHL and ML was observed. We therefore assumed that the interaction of ML seemed to be the likely cause of the reduced stretching ability of solutions and thus increasing the fiber diameter. ML might interact with the SHL by intercalating among the polymeric chains and thus impeding the elongation or stretching capacity (as postulated in Fig. 7). Additionally, the slight decrease of solution conductivity as increasing ML contents also reduced the charge density of electrospun solutions leading to the impaired elastic force within the jet [20]. Nevertheless, the impacts of applied voltage and feed rate on the fiber morphology tended to be not important as apparently displayed below the t value limit (Fig. 5).

The occurrence of beads on the electrospun fibers is considered as defect. As indicated by Pareto chart in Fig. 5B, only

Table 4 – Results of ANOVA for different responses.

Responses	Coefficients	P value	Std. Dev.	% CV	Mean value	R <sup>2</sup>	F value
Y <sub>1</sub> (nanofiber diameter)			106.87	19.68	542.89	0.7480	
X <sub>1</sub>	173.81	<0.0001					
X <sub>2</sub>	60.69	0.0373					
Intercept	542.89						
Model		<0.0001					23.74
Lack of fit		0.1157					8.06
Y <sub>2</sub> (bead amount)			0.22	45.08	0.48	0.7527	
X <sub>1</sub>	-0.39	<0.0001					
Intercept	0.48						
Model		<0.0001					51.73
Lack of fit		0.0827					11.52

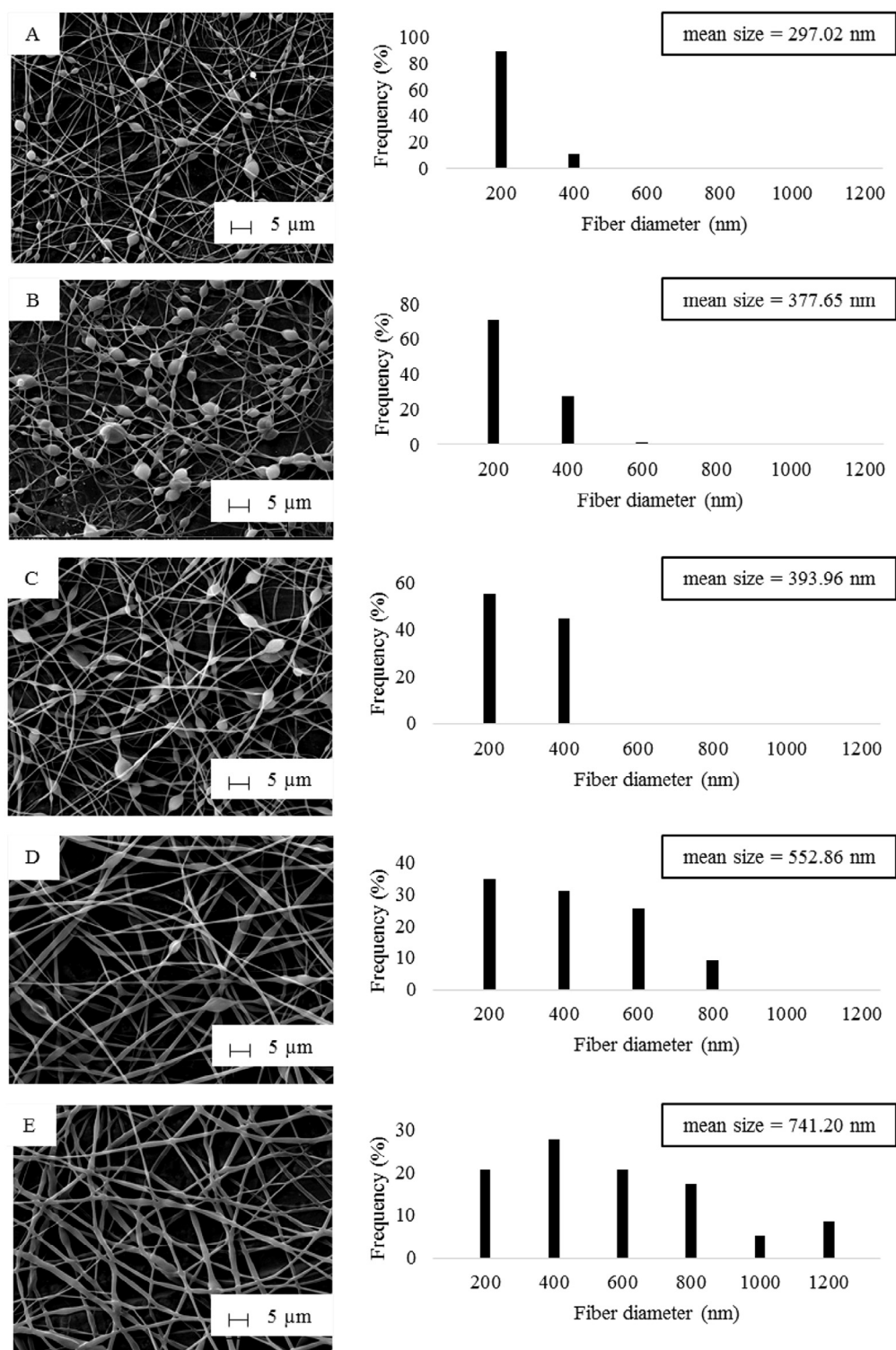
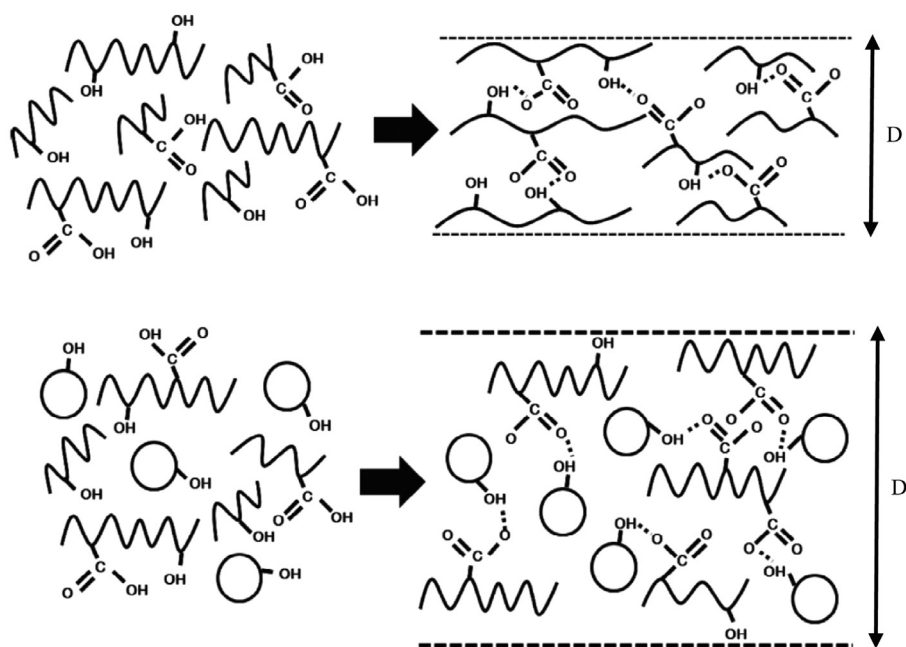


**Fig. 6** – SEM images and diameter distribution of SHL-ML nanofibers at the weight ratio of (A) 35: 1, (B) 35: 3, (C) 37.5: 2, (D) 40: 1 and (E) 40: 3.

the content of SHL ( $X_1$ ) had a remarkable impact on the appearance of beads. The number of beads had a tendency to decrease with increasing concentration of SHL while the smooth fibers were obtained from 40% w/w SHL and 3% w/w ML (Fig. 6). Based on Table 2, an increase in the viscosity of SHL might

lead to the high interaction between the polymers and solvent molecules. The aggregation probability of the solvent molecules was thus reduced. As a result, the beaded fibers were gradually changed to smooth fibers [20]. In order to predict the impact of independent factors on the diameter of fiber



### Solutions

Fig. 7 – Schematic diagram representing the influence of ML on fiber diameter.

( $Y_1$ ) and the amount of bead ( $Y_2$ ) represented by bead-to-fiber ratio, mathematical models were performed as presented in the following equations. The Equation 2 and 3 referred to actual factors with  $R^2$  values of 0.7480 and 0.7527, respectively indicating the good fit of the model.

$$\text{Diameter} = 69.525(\text{SHL content}) + 60.6875(\text{ML content}) - 2185.66776. \quad (2)$$

$$\text{Bead amount} = 6.37171 - 0.157(\text{SHL content}). \quad (3)$$

According to the results of ANOVA shown in Table 4, the prediction of the models would be reliable referring to the

$P$  values of the models which were less than 0.05. Moreover, the lack of fit was not significant with  $P$  values of 0.1157( $Y_1$ ) and 0.0827( $Y_2$ ) indicating that these models were suitable. The coefficients represented the magnitude and direction of the factor effects. As presented in Table 4, SHL content ( $X_1$ ) was the most influential parameter on the nanofiber diameter and bead amount with positive and negative relationships respectively, corresponding to the results from Pareto diagrams (Fig. 5) and two-dimensional contour plots (Fig. 8) which were also displayed in order to estimate the effect of each factor on the responses. Based on Fig. 8A, the small fibers could be gen-

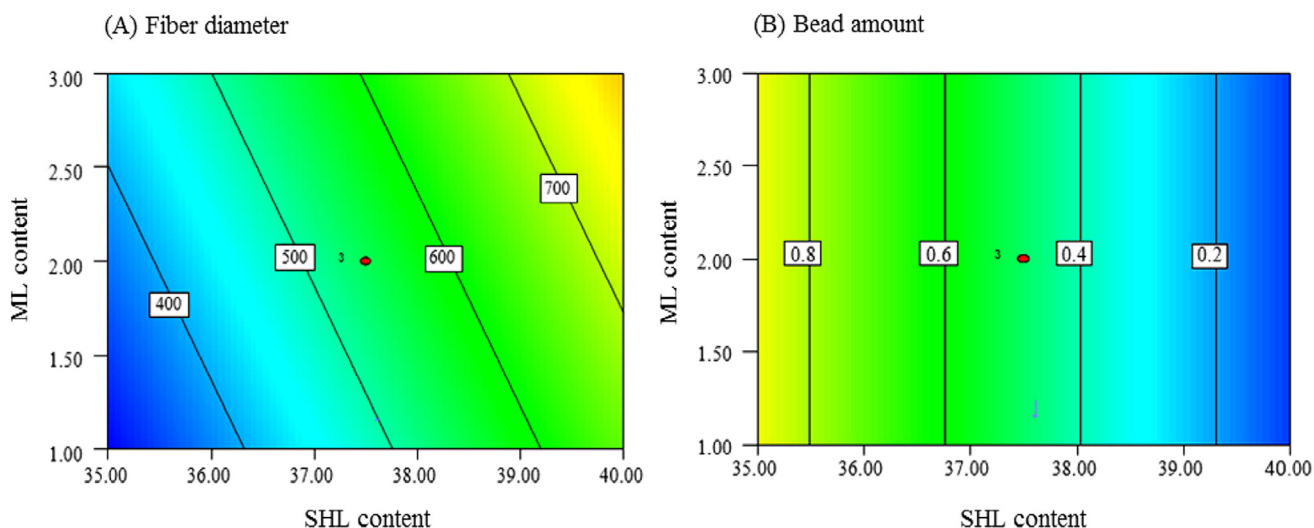


Fig. 8 – Two-dimensional contour plots presenting the effects of SHL and ML contents on (A) fiber diameter and (B) bead amount.

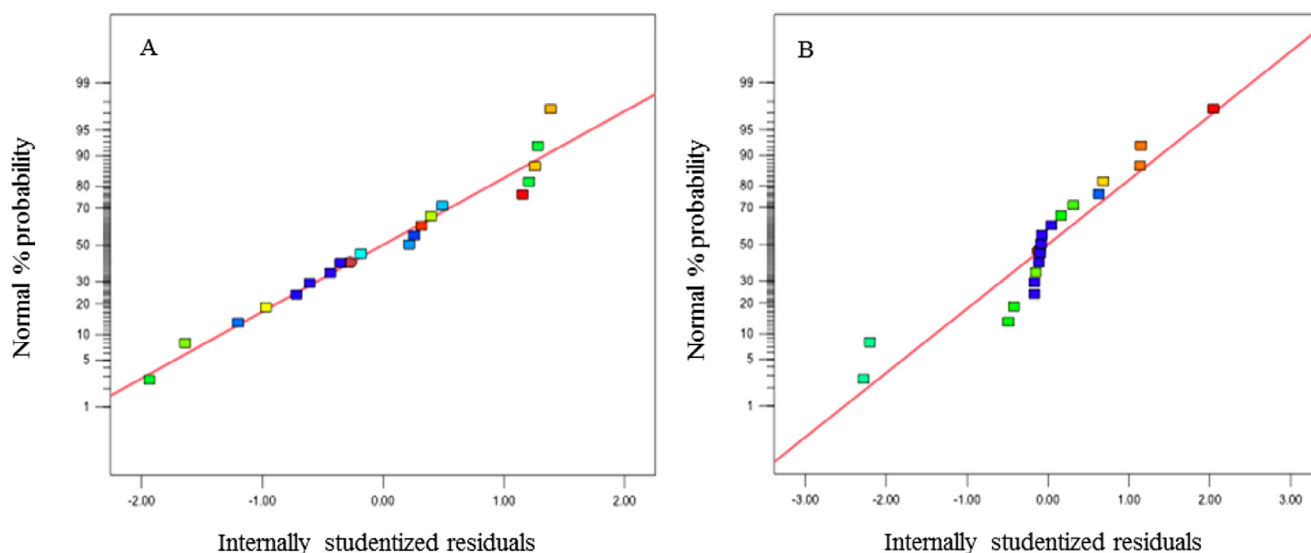


Fig. 9 – Normal probability plots of nanofiber (A) diameter and (B) bead amount.

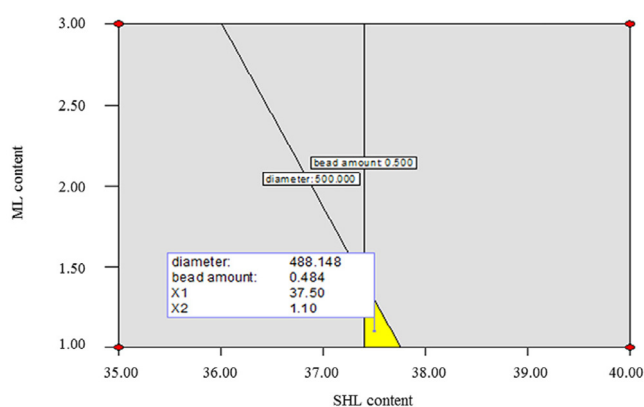


Fig. 10 – Overlay plot for optimization of SHL nanofibers loaded with ML.

erated from the low amounts of SHL and ML. Meanwhile, the beadless fibers might be obtained from the high concentration of SHL regardless of the amount of SHL as depicted in Fig. 8B.

The normal probability plots of residuals are illustrated in order to explain the validity of the obtained data. Referring to Fig. 9A and 9B, the residuals seemed to fit a straight line indicating that the errors were normally distributed; thus, the data were acceptable.

### 3.3.2. Optimization of SHL-ML nanofibers

The graphical model was presented with the aim of exploring the optimal region leading to the fabrication of the desired nanofibers. There are two types of the represented graph which are generally displayed as the three-dimensional response surface and the contour plot illustrated by the plane surface [28]. In this study, an overlay contour plot was depicted as shown in Fig. 10. The chosen desirable ranges of fiber diameter and bead-to-fiber ratio were 300–500 nm and 0–0.5, respectively. Based on the overlay plot, the example of the opti-

imum conditions for the fabrication of SHL-ML nanofibers with thinner diameter (488 nm) and beadless (0.48) was attained at the SHL and ML contents of 37.5% and 1.1% w/w respectively, with the applied voltage of 18 kV and the flow rate of 0.8 ml/h.

### 3.4. Time-kill kinetic study

In this work, time-kill kinetic study was carried out in order to determine the pharmacodynamics of ML, providing a profile of antimicrobial effect against *S. aureus*, *E. coli* and *C. albicans* which represented Gram-positive and Gram-negative bacteria and fungi, respectively, at different time periods. The percentage of living cells of *S. aureus*, *E. coli* and *C. albicans* over a period of time was presented in Fig. 11. With regard to Fig. 11A, the number of *S. aureus* exposed to SHL-ML nanofibers gradually decreased as compared to those treated with ML solution which provided immediate killing potential, estimating that the release of ML from SHL nanofibers was dependent on the solubility of SHL in liquid media. Thus, the antibacterial action of SHL-ML nanofibers tended to be relatively sustained. The mode of action was previously reported. ML, a lipophilic compound, might be accumulated into the membrane bilayer, and consequently disintegrates the microbial membrane by fluidizing the lipids and phospholipids in the envelope of the organism, changing of the hydrogen bonding and the dipole-dipole interaction between acyl chains exerting bactericidal effects [14].

Nevertheless, many studies reported that *E. coli* was found to be less affected by ML [29]. The difference in the killing effects of lipids against Gram-negative bacteria might depend on the differences in the outer membrane. Based on the structure of *E. coli*, the external membrane consists of proteins and lipopolysaccharides (LPS) which are composed of the O-polysaccharide chains demonstrating a hydrophilic surface property. Therefore, lipids, which are hydrophobic molecules, could have difficulty in entering the bilayer, and be hardly diffused in the cytoplasm [30,31]. This was consistent with the

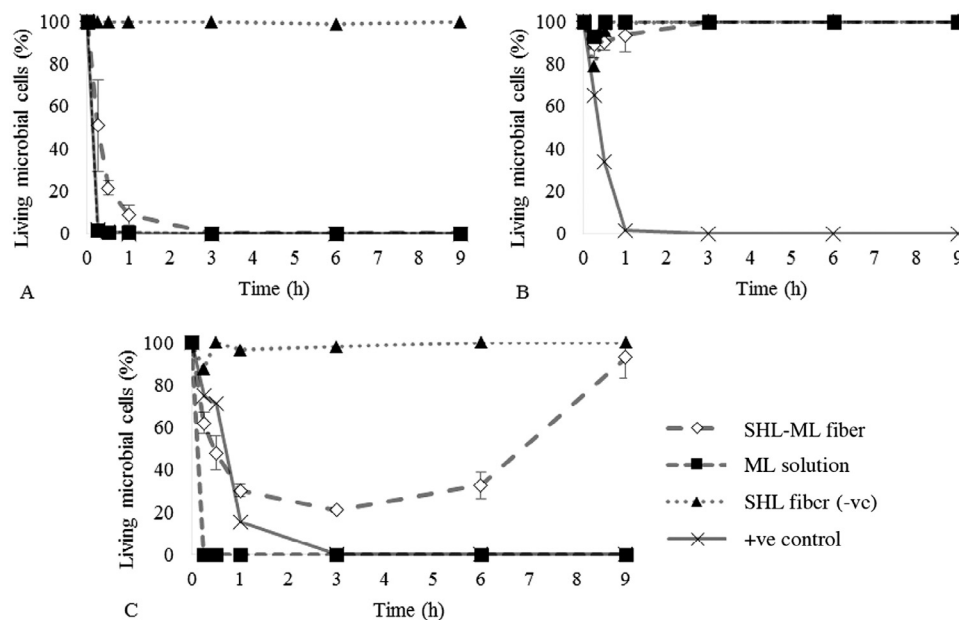


Fig. 11 – Kill kinetics of nanofibers for (A) *S. aureus*, (B) *E. coli* and (C) *C. albicans* over a period of 9 h.

result as shown in Fig. 11B. Both of SHL nanofibers loaded with ML and ML solution did not display activity against *E. coli*. The number of living cells was significantly increased over time.

As mentioned before, ML also has an antifungal effect by inhibiting spore germination and preventing the radial growth [17]. Fig. 11C demonstrated that some of *C. albicans* were killed by the ML released from fibers. However, after a period of 3 h, the amount of *C. albicans* then slightly increased, while the number of *C. albicans* exposed to ML in a solution form obviously declined without re-increasing. This might be explained by the effect of pH media on the solubility of SHL. According to the study of Limmatvapirat et al. [32], SHL with a  $pK_a$  of 6.9–7.5 could be dissolved at pH above 7. Therefore, the solubility limitation of SHL in SDB media, which has an approximate pH value of 5.6, might occur. The release of ML from SHL carrier seemed to be incomplete which was due to the low pH of the liquid medium. During the initial period of exposure, only some of ML, especially at the surface of nanofibers was rapidly released and partially eradicated the *C. albicans* while most of ML was expected to be trapped in the SHL matrix and slowly released which was considered as the prolonged exposure time. As a result, the concentration of ML was not enough to inhibit the regrowth of living microorganisms after a 3-h exposure to SHL-ML nanofibers. Thus, the application of SHL-ML nanofibers in chronic wound management might be effective due to the predominant alkaline pH of chronic wounds (7.1–8.9), while treatment of acute wounds, which have low pH values of 5–6, seems to be restricted [33].

#### 4. Conclusion

SHL nanofibers loaded with ML could be developed for wound dressing application in order to prevent the delayed wound healing resulting from microbial infection. The main and in-

teraction effects of factors on the morphology of nanofibers were investigated by using a full factorial design with three replicated center points. According to the results, the SHL content was the major parameter affecting the fiber diameter, while the loaded ML content might be the minor parameter. The study of parameters on bead amount was evaluated revealing that the SHL content was the most significant negative impact on bead amount. The optimum conditions for the fabrication of small and beadless nanofibers were studied. The desired fibers could be obtained at the SHL and ML concentrations of 37.5% and 1.1% w/w respectively, with the applied voltage of 18 kV and the flow rate of 0.8 ml/h. Moreover, time–kill assays were performed in order to study the pharmacodynamics of antimicrobial agents, showing a profile of antimicrobial activity over time. The results showed that SHL nanofibers loaded with ML provided an excellent antibacterial activity against *S. aureus* whereas *E. coli* was less affected. ML also exhibited antifungal effect against *C. albicans*. However, the release of ML might depend on the solubility of SHL carrier. Therefore the effect of pH in wound environment was considerable. The application of SHL-ML nanofibers in chronic wound management might be effective due to the predominant alkaline pH of chronic wounds, while treatment of acute wounds, which have low pH values, seems to be restricted.

#### Conflicts of interest

The authors declare that there is no conflict of interest.

#### Acknowledgements

The authors acknowledge the financial support received from Silpakorn University Research and Development Institute.

The study was also supported by the Higher Education Research Promotion and National Research University Project of Thailand, Office of the Higher Education Commission (2559A11462006); and Faculty of Pharmacy, Silpakorn University.

## REFERENCES

- [1] Abdelrahman T, Newton H. Wound dressings: principles and practice. *Surgery* 2011;29:491–5.
- [2] Stashak TS, Farstvedt E, Othic A. Update on wound dressings: indications and best use. *Clin Tech Equine Pract* 2004;3:148–63.
- [3] Engel E, Michiardi A, Navarro M, Lacroix D, Planell JA. Nanotechnology in regenerative medicine: the materials side. *Trends Biotechnol* 2008;26:39–47.
- [4] Pelipenko J, Kocbek P, Govedarica B, Rošic R, Baumgartner S, Kristl J. The topography of electrospun nanofibers and its impact on the growth and mobility of keratinocytes. *Eur J Pharm Biopharm* 2013;84:401–11.
- [5] Unnithan AR, Gnanasekaran G, Sathishkumar Y, Lee YS, Kim CS. Electrospun antibacterial polyurethane-cellulose acetate-zein composite mats for wound dressing. *Carbohydr Polym* 2013;102:884–92.
- [6] Hu X, Liu S, Zhou G, Huang Y, Xie Z, Jing X. Electrospinning of polymeric nanofibers for drug delivery applications. *J Control Release* 2014;185:12–21.
- [7] Thammachat T, Sriamornsak P, Luangtana-Anan M, Nunthanid J, Limmatvapirat C, Limmatvapirat S. Preparation and characterization of shellac fiber as a novel material for controlled drug release. *Adv Mat Res* 2010;152–153:1232–5.
- [8] Okamoto MY, Ibanez PS. Final report on the safety assessment of shellac. *J Am Coll Toxicol* 1986;5:309–27.
- [9] Alzahrani H, Bedir Y, Al-Hayani A. Efficacy of shellac, a natural product, for the prevention of wet gangrene. *J Int Med Res* 2013;41:795–803.
- [10] Porter SC. Coating of pharmaceutical dosage forms. In: Lieberman HA, editor. *Pharmaceutical dosage forms: tablet*. New York: Marcel Dekker Inc.; 1990. p. 77–160.
- [11] Thormar H, Hilmarsen H. The role of microbicidal lipids in host defense against pathogens and their potential as therapeutic agents. *Chem Phys Lipids* 2007;150:1–11.
- [12] Isaacs CE, Litov RE, Thormar H. Antimicrobial activity of lipids added to human milk, infant formula, and bovine milk. *Nutr Biochem* 1995;6:362–6.
- [13] Lieberman S, Enig MG, Preuss HG. A review of monolaurin and lauric acid: natural virucidal and bactericidal agents. *Altern Complement Ther* 2006;12:310–14.
- [14] Tangwatcharin P, Khopaibool P. Activity of virgin coconut oil, lauric acid or monolaurin in combination with lactic acid against *Staphylococcus aureus*. *Southeast Asian J Trop Med Public Health* 2012;43:969–85.
- [15] Nobmann P, Smith A, Dunne J, Henahan G, Bourke P. The antimicrobial efficacy and structure activity relationship of novel carbohydrate fatty acid derivatives against *Listeria* spp. and food spoilage microorganisms. *Int J Food Microbiol* 2009;128:440–5.
- [16] Carpo BG, Verardo-Rowell VM, Kabara JJ. Novel antibacterial activity of monolaurin compared with conventional antibiotics against organisms from skin infections: an in vitro study. *J Drugs Dermatol* 2007;6:991–8.
- [17] Rihakova Z, Filip V, Plockova M, Smidrkal J, Cervenkova R. Inhibition of *Aspergillus niger* DMF 0801 by monoacylglycerols prepared from coconut oil. *Czech J Food Sci* 2002;20:48–52.
- [18] Schlievert PM, Peterson ML. Glycerol monolaurate antibacterial activity in broth and biofilm cultures. *PLoS ONE* 2012;7:1–12.
- [19] Selem D, Chen E, Benso B, Pardi V, Murata RM. In vitro evaluation of antifungal activity of monolaurin against *Candida albicans* biofilms. *PeerJ* 2016;4:1–17.
- [20] Ramakrishna S, Fujihara K, Teo WE, Lim TC, Ma Z. An introduction to electrospinning and nanofibers. Singapore: World Scientific Publishing; 2005.
- [21] Montgomery DC. Design and analysis of experiments. 7th ed. New York: John Wiley & Sons; 2009.
- [22] Dooren AAV. Design for drug-excipient interaction studies. *Drug Dev Ind Pharm* 1983;9:43–55.
- [23] Chen X, Wu D, He Y, Liu S. Detecting the quality of glycerol monolaurate: a method for using Fourier transform infrared spectroscopy with wavelet transform and modified uninformative variable elimination. *Anal Chim Acta* 2009;638:16–22.
- [24] Limmatvapirat S, Panchapornpon D, Limmatvapirat C, Nunthanid J, Luangtana-Anan M, Puttipipatkachorn S. Formation of shellac succinate having improved enteric film properties through dry media reaction. *Eur J Pharm Biopharm* 2008;70:335–44.
- [25] Mishra MK. Solution properties of shellac, 4. Solubility parameter of shellac. *Macromol Mater Eng* 1987;147:107–12.
- [26] Blaszyk M, Holley RA. Interaction of monolaurin, eugenol and sodium citrate on growth of common meat spoilage and pathogenic organisms. *Int J Food Microbiol* 1998;39:175–83.
- [27] Dhekale NH, Bindu KH, Kirankumar KY, Gore AN, Anbhule PV, Kolekar GB. Development and optimization of a multivariate RP-UPLC method for determination of telmisartan and its related substances by applying a two-level factorial design approach: application to quality control study. *Anal Methods* 2014;6:5168–82.
- [28] Candiotti LV, De Zan MM, Camara MS, Cámara MS, Goicoechea HC. Experimental design and multiple response optimization. Using the desirability function in analytical methods development. *Talanta* 2014;124:123–38.
- [29] Skrivanova E, Marounek M, Benda V, Brezina P. Susceptibility of *Escherichia coli*, *Salmonella* sp. and *Clostridium perfringens* to organic acids and monolaurin. *Vet Med (Praha)* 2006;51:81–8.
- [30] Bergsson G, Steingrimsson O, Thormar H. Bactericidal effects of fatty acids and monoglycerides on *Helicobacter pylori*. *Int J Antimicrob Agents* 2002;20:258–62.
- [31] Ouattara B, Simard RE, Holley RA, Piette GJ, Bégin A. Antibacterial activity of selected fatty acids and essential oils against six meat spoilage organisms. *Int J Food Microbiol* 1997;37:155–62.
- [32] Limmatvapirat S, Limmatvapirat C, Luangtana-Anan M, et al. Modification of physicochemical and mechanical properties of shellac by partial hydrolysis. *Int J Pharm* 2004;278:41–9.
- [33] Schneider LA, Korber A, Grabbe S, Dissemmond J. Influence of pH on wound healing: a new perspective for wound therapy. *Arch Dermatol Res* 2007;298:413–20.